WestVirginiaUniversity
THE RESEARCH REPOSITORY @ WVU

Faculty Scholarship

2015

Phase-Lag Synchronization In Networks Of Coupled Chemical Oscillators

Jan F. Totz

Razan Snari

Desmond Yengi

Mark R. Tinsley

Harald Engel

See next page for additional authors

Follow this and additional works at: https://researchrepository.wvu.edu/faculty_publications

Digital Commons Citation

Totz, Jan F.; Snari, Razan; Yengi, Desmond; Tinsley, Mark R.; Engel, Harald; and Showalter, Kenneth, "Phase-Lag Synchronization In Networks Of Coupled Chemical Oscillators" (2015). *Faculty Scholarship*. 631.
https://researchrepository.wvu.edu/faculty_publications/631

This Article is brought to you for free and open access by The Research Repository @ WVU. It has been accepted for inclusion in Faculty Scholarship by an authorized administrator of The Research Repository @ WVU. For more information, please contact ian.harmon@mail.wvu.edu.

Authors
Jan F. Totz, Razan Snari, Desmond Yengi, Mark R. Tinsley, Harald Engel, and Kenneth Showalter

This article is available at The Research Repository @ WVU: https://researchrepository.wvu.edu/faculty_publications/631

Phase-lag synchronization in networks of coupled chemical oscillators

Jan F. Totz,[1] Razan Snari,[2] Desmond Yengi,[2] Mark R. Tinsley,[2] Harald Engel,[1] and Kenneth Showalter[2,*]
[1]*Institut für Theoretische Physik, EW 7-1, TU Berlin, Hardenbergstr. 36, D-10623 Berlin, Germany*
[2]*C. Eugene Bennett Department of Chemistry, West Virginia University, Morgantown, West Virginia 26505-6045, USA*
(Received 9 December 2014; published 27 August 2015)

Chemical oscillators with a broad frequency distribution are photochemically coupled in network topologies. Experiments and simulations show that the network synchronization occurs by phase-lag synchronization of clusters of oscillators with zero- or nearly zero-lag synchronization. Symmetry also plays a role in the synchronization, the extent of which is explored as a function of coupling strength, frequency distribution, and the highest frequency oscillator location. The phase-lag synchronization occurs through connected synchronized clusters, with the highest frequency node or nodes setting the frequency of the entire network. The synchronized clusters successively "fire," with a constant phase difference between them. For low heterogeneity and high coupling strength, the synchronized clusters are made up of one or more clusters of nodes with the same permutation symmetries. As heterogeneity is increased or coupling strength decreased, the phase-lag synchronization occurs partially through clusters of nodes sharing the same permutation symmetries. As heterogeneity is further increased or coupling strength decreased, partial synchronization and, finally, independent unsynchronized oscillations are observed. The relationships between these classes of behavior are explored with numerical simulations, which agree well with the experimentally observed behavior.

DOI: 10.1103/PhysRevE.92.022819 PACS number(s): 82.40.Qt, 05.45.−a

I. INTRODUCTION

Synchronization lies at the heart of a wide range of physical, chemical, and biological phenomena [1–3]. Synchronization in networks is currently the focus of extensive research aimed at developing a better understanding of networks of interacting dynamical elements [4–12]. Biological systems offer particularly compelling examples of network synchronization [13]; for example, central pattern generators (CPG) are known to produce and control rhythmic behavior such as breathing and movement [14]. We now know that the swimming motion of the lamprey fish is controlled by a CPG that emits subsequent phase waves, entraining the neuronal network of the spinal cord [15].

Although theoretical studies have provided many of the advances in research on network synchronization [4–12], a number of experimental studies of physical and chemical networks have now been reported. Experiments on systems of coupled lasers [16,17], electro-optic devices [18], electrochemical oscillators [19–21], and Belousov-Zhabotinsky oscillators [22–25] have provided insights into network synchronization in real-world settings. Recently, a study by Pecora *et al.* [26] demonstrated the importance of permutation symmetries in zero-lag synchronization, which was also shown experimentally with an electro-optic network. The permutation symmetries allow the master stability function for the complete network to be decomposed into subunits.

Here we address the question: What role does symmetry play when the oscillator heterogeneity is sufficiently large that phase-lag synchronization [3] is exhibited? A versatile experimental system for investigating the synchronization dynamics of coupled oscillators is the Belousov-Zhabotinsky (BZ) reaction [27]. Individual chemical oscillators are generated by placing cation exchange beads loaded with the BZ catalyst into catalyst-free BZ reaction mixtures [28]. This modified BZ system has been used to study diffusively coupled oscillators [29] and synchronization transitions in globally coupled systems [30,31]. The photosensitive BZ reaction, with the catalyst $Ru(bipy)_3^{2+}$ [32,33], allows a wide range of network topologies and coupling schemes to be realized, where the coupling is through photochemical feedback [23,24,34]. Color changes arising from the concentration of the reduced catalyst $Ru(bipy)_3^{2+}$ (orange) and its oxidized form $Ru(bipy)_3^{3+}$ (green) allow the phase of an oscillator to be determined by grayscale measurements with a CCD camera. The photochemical feedback occurs by the illumination of each bead with a spatial light modulator (SLM) at 460 nm, which leads to the production of $HBrO_2$, the autocatalyst of the BZ reaction [23,34–36].

In this paper, we report on studies of networks of BZ chemical oscillators with bidirectional coupling, defined by the adjacency matrix A_{ij}, consisting of N oscillators with a distribution of periods. The oscillators are coupled by a linear interaction function of the normalized grayscale value difference $(z_j - z_i)$ without delay or phase frustration. We calculate the feedback light intensity ϕ_i to the i^{th} node as

$$\phi_i = \phi_0 + \frac{\sigma}{k_i} \sum_{j=1}^{N} A_{ij}(z_j - z_i), \tag{1}$$

where ϕ_0 is the background intensity, and the coupling strength σ is normalized by the degree k_i of the respective node. The normalized grayscale values z_i and z_j for nodes (oscillators) i and j are obtained from the transmitted light intensity of the oscillators and are proportional to the concentration of $Ru(bipy)_3^{3+}$. Equation (1) is used to calculate the feedback light intensity ϕ_i with the ZBKE model [37] for the photosensitive BZ reaction (see Supplemental Material [38]) in the simulations described below.

The oscillator with the highest frequency plays a special role in systems of coupled heterogeneous oscillators [39]. Depending on the coupling strength and frequency heterogeneity, it may dictate the frequency of all the oscillators (complete

*kenneth.showalter@mail.wvu.edu

 ©2015 American Physical Society

synchronization), only of a subset (partial synchronization) or none of the oscillators (incoherence) [40]. The symmetry properties of the network are also of key importance in the coupled oscillator dynamics [26]. Networks exhibit permutation symmetries [41] rather than Euclidean symmetries, such as reflection, rotation, and translation. Permutations exchange up to N node positions in the network. The action of a symmetric permutation P commutes with the adjacency matrix A, $PA = AP$. The network symmetries or automorphisms can be readily computed with computer algebra software [26,42]. A spatial representation of a network may possess spatial symmetries that reflect the underlying permutation symmetries; however, this occurs only for specifically tailored node positioning [41].

All experiments are conducted with the following protocol: The initial conditions are prepared by imposing global coupling between all oscillators for 200 s. The system is then changed from global coupling to the specific network topology, as shown in Fig. 1(a). The unperturbed period is measured at the conclusion of the experiment after removing the photochemical coupling of the oscillators.

We first describe experiments in which phase-lag synchronization of a network of chemical oscillators occurs through *symmetry clusters*, which are clusters of nodes with the same permutation symmetries. We then describe phase-lag synchronization that occurs only partially through these clusters, as coupling strength is decreased or frequency heterogeneity is increased. The location of the highest frequency oscillator may also play an important role in this behavior. On further decreasing coupling strength or increasing frequency heterogeneity, the frequency synchronization of the network breaks down until finally only unsynchronized oscillators are observed. We then present simulations of the chemical oscillator network in which the synchronization behavior is examined as a function of coupling strength and frequency heterogeneity. The simulations reveal a transition from phase-lag synchronization through symmetry clusters to synchronization partially through symmetry clusters to partial synchronization to unsynchronized behavior as the coupling strength is decreased or the frequency heterogeneity is increased.

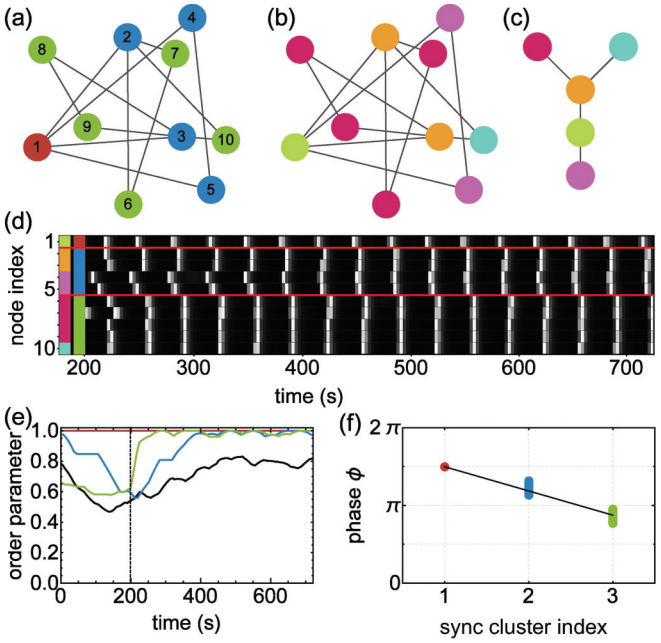

FIG. 1. (Color) Phase-lag synchronization in a network of Belousov-Zhabotinsky (BZ) chemical oscillators. (a) The bidirectional links show the connectivity in the network. Nodes that oscillate simultaneously, or nearly so, define a *synchronization cluster* and are the same color. (b) Nodes that have the same permutation symmetries define a *symmetry cluster* and are the same color. (c) A reduced representation of the symmetry clusters. (d) Experimentally recorded grayscale values of all oscillators, showing the wave pattern. The node index corresponds to the numbering in (a). Red lines separate the synchronization clusters, with the synchronization clusters and symmetry clusters color coded (at left) as in (a) and (b), respectively. (e) Kuramoto order parameter [2] for each synchronization cluster, color coded as in (a), and the complete network (black) as a function of time. The network connections are established at 200 s (dashed line) following initial conditions of frequency synchronization with global coupling. (f) A linear fit through the phase occurrence of each node of each synchronization cluster reveals a constant phase difference between synchronization clusters [color coding as in (a)]. Note that the synchronization cluster index is equivalent to the network distance from the pacemaker with an offset of 1. See the Supplemental Material [38] for experimental setup and parameters as well as five other network topologies. Average natural period and standard deviation $T_0 = 35.02 \pm 1.10$ s; coupling strength $\sigma = 2.0$.

II. PHASE-LAG SYNCHRONIZATION THROUGH SYMMETRY CLUSTERS

When the nodes are sorted according to their temporal firing sequence, a pattern of phase-lag synchronization emerges, which is described in Fig. 1. The experimentally measured gray level for each oscillator as a function of time, with the node index given in Fig. 1(a), is shown in Fig. 1(d). As the network begins to synchronize at approximately 400 s, the nodes fire in sequence, with node 1 firing first, nodes 2–5 firing next, and finally nodes 6–10 firing last, and the cycle then repeats for the remainder of the experiment. The nodes that fire nearly simultaneously define a *synchronization cluster*, each of which is color coded (at left) in Fig. 1(d) as in Fig. 1(a). The *symmetry clusters* of the network, which are determined only by the node connectivities, ignoring the oscillator heterogeneity, are indicated in Fig. 1(b) by a different color coding, which is also shown (at left) in Fig. 1(d). On comparing Figs. 1(a) and 1(b), two features become apparent: Each synchronization cluster is made up of symmetry clusters, and any particular synchronization cluster may include more than one symmetry cluster. This can also be seen by comparing the color-coded nodes of the symmetry clusters and synchronization clusters in Fig. 1(d).

In order to characterize the degree of synchronization of the synchronization clusters, we determine the Kuramoto order parameter [2] for each synchronization cluster as a function of time, as shown in Fig. 1(e). We see that the order parameter for the first synchronization cluster (node 1, red) is trivially equal to 1.0; however, the order parameter for second (blue) and third (green) synchronization clusters is very close to 1.0 after the network synchronizes. The order parameter as a function

of time is also determined for the entire network, which is shown by the black curve. We see that the value of the order parameter for the network does not approach 1.0, because of the phase lag between the synchronization clusters.

To characterize the phase lag between each synchronization cluster, we plot the phase when each node fires in each synchronization cluster relative to when the first synchronization cluster (node 1) fires, as shown in Fig. 1(f). To obtain the relative phases, we set the phase when the first synchronization cluster fires to $3\pi/2$. The occurrence plot in Fig. 1(f) shows that there is a constant phase difference between the firing of the nodes in the first and second synchronization clusters and between the firing of the nodes in the second and third synchronization clusters, as indicated by the linear fit. Any two oscillators can be considered to be entrained if their phase difference $\Delta\phi$ is bounded [3], and in our experiments we find $0.5 < \Delta\phi < 1.35$ for the phase difference between synchronization clusters, where a lower bound is included to distinguish between phase-locked states with zero and nonzero phase differences.

We note that phase-lag synchronization through synchronization clusters made up of symmetry clusters, as described in Fig. 1, is observed with other network topologies of coupled heterogeneous chemical oscillators. We analyze the phase-lag synchronization in simulations of five different networks of coupled BZ oscillators in the Supplemental Material [38]. The simulations reveal highly synchronized clusters in plots similar to Figs. 1(d) and 1(e), and a constant phase lag between the synchronization clusters in plots similar to Fig. 1(f). We also present an analysis of the period of the synchronized network, with topology as in Fig. 1(a), and the natural periods of the uncoupled oscillators. In simulations with five different frequency distributions, we find that the period of the synchronized network and the natural period of the highest frequency uncoupled oscillator, which serves as the pacemaker for the network, differ by less than 1%.

When phase-lag synchronization occurs through synchronization clusters that are made up of symmetry clusters, as in Fig. 1, it is possible to simplify the network by replacing each symmetry cluster with a single composite node. In Figs. 1(b) and 1(c), we show how the network of 10 nodes is reduced to five nodes. The simpler network in Fig. 1(c) exhibits the same frequency and phase synchronization properties as the full network in Fig. 1(b). In this example, the green symmetry cluster (node 1) fires first, which is connected to the violet (nodes 2 and 3) and orange (nodes 4 and 5) symmetry clusters, which fire next. The orange symmetry cluster is connected to the red (nodes 6–9) and blue (node 10) symmetry clusters, which fire next, and the cycle then repeats. This reduction allows the phase-lag synchronization dynamics to be predicted regardless of which symmetry cluster or clusters become the pacemaker. The approach allows large and complex networks to be reduced to simpler but equivalent analogs.

III. PHASE-LAG SYNCHRONIZATION PARTIALLY THROUGH SYMMETRY CLUSTERS

Figure 2 shows an example of phase-lag synchronization that occurs only partially through the symmetry clusters. This behavior occurs when the pacemaker site, a synchronization

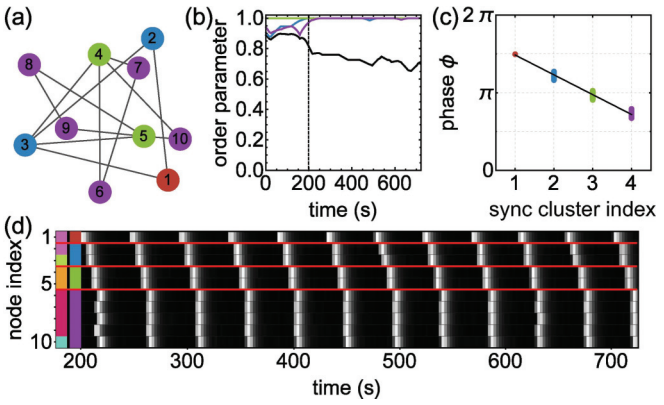

FIG. 2. (Color) Phase-lag synchronization that occurs only partially through symmetry clusters. (a) and (d) Because the pacemaker (node 1) is not a complete symmetry cluster, as in Fig. 1, the red and blue synchronization clusters do not correspond to the symmetry clusters in Fig. 1(b). (b) Kuramoto order parameter [2] for each synchronization cluster, color coded as in (a), and the complete network (black) as a function of time. (c) A linear fit through the phase occurrence of each node of each synchronization cluster [color coding as in (a)]. Average natural period and standard deviation $T_0 = 50.59 \pm 3.81$ s; coupling strength $\sigma = 2.0$. Other parameters as in Fig. 1.

cluster of one or more oscillators, does not include an entire symmetry cluster. The measured gray level for each oscillator as a function of time is shown in Fig. 2(d), with the node index given in Fig. 2(a). After the network synchronizes at approximately 250 s, we again see the nodes firing in sequence, with node 1 firing first, nodes 2 and 3 firing next, nodes 4 and 5 firing next, and finally nodes 6–10 firing last. This cycle then repeats for the remainder of the experiment. An examination of the synchronization clusters, which are color coded in Fig. 2(a) and indicated (at left) in Fig. 2(d), and the symmetry clusters, which are color coded in Fig. 1(b) and also indicated (at left), shows that the first synchronization cluster (red, node 1) is only part of the violet symmetry cluster, and that the second synchronization cluster (blue) is made up of part of the violet symmetry cluster and the green symmetry cluster. However, because the green symmetry cluster is fully connected to the orange symmetry cluster, the third synchronization cluster (green) is made up of the orange symmetry cluster. Hence, the phase-lag synchronization through the symmetry clusters is regained, and the fourth synchronization cluster (purple) is made up of the red and light blue symmetry clusters. Even though phase-lag synchronization occurs only partially through symmetry clusters in this example, the synchronization is robust for over 35 periods. For phase-lag synchronization to completely occur through symmetry clusters, it is necessary for the pacemaker to connect to all nodes of one or more symmetry clusters.

Figure 2(b) shows the Kuramoto order parameter [2] for each synchronization cluster as a function of time. We see a high degree of zero-lag phase synchronization in each of the synchronization clusters, with the order parameter for each approaching 1.0. The order parameter for the entire network, shown by the black curve, does not approach 1.0 because of the phase difference between each of the synchronization clusters.

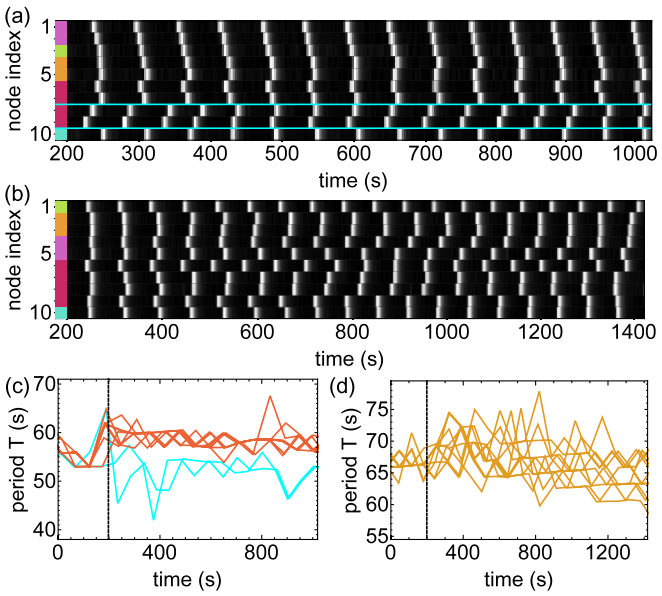

FIG. 3. (Color online) Network dynamics without complete synchronization. (a) and (c) Frequency synchronization in two groups of oscillators: nodes 1–7 and 10 and nodes 8 and 9 (separated by horizontal lines). Average natural period and standard deviation $T_0 = 55.65 \pm 8.62$ s; coupling strength $\sigma = 0.60$. (b) and (d) No synchronization occurs at low coupling strength, and a broad distribution in period is exhibited. Average natural period and standard deviation $T_0 = 55.97 \pm 2.04$ s; coupling strength $\sigma = 0.05$. Other parameters as in Fig. 1.

Figure 2(c) shows an occurrence plot of the phase at which each node in each synchronization cluster fires relative to when the pacemaker, node 1, fires. A constant phase difference between the firing of the nodes in each synchronization cluster is indicated by the linear fit.

IV. PARTIAL SYNCHRONIZATION AND LOSS OF SYNCHRONIZATION

Frequency synchronization between two coupled oscillators is ensured only when the ratio of the frequency difference to the coupling strength is sufficiently small [3]. This condition is violated for small coupling strengths or large widths of the frequency distribution. Pairwise frequency entrainment of neighboring nodes i and j will gradually disappear in saddle-node bifurcations [2], depending on the frequency detuning $\Delta\omega_{ij}$ and the maximum of the antisymmetric (odd) part of the interaction function [43]. In this case, we observe only partial frequency synchronization, as shown in Fig. 3(a). The oscillators divide into two groups with different frequencies, $\omega_1 = 0.11$ Hz (period 57 s) and $\omega_2 = 0.12$ Hz (period 52 s), as shown in Fig. 3(c). Both groups become aligned due to beating, with a minimum average phase difference between the nodes occurring approximately every 10 periods of the faster group. We note that synchronization clusters do not appear, and there seems to be no relation between the oscillator phases and the symmetry clusters. As expected, even partial frequency synchronization disappears on further reducing the coupling strength, Figs. 3(b) and 3(d), and no periods align. The phase difference between any two oscillators grows without bound, and any entrainmentlike phase distribution is short-lived and occurs only as a result of beating.

V. NUMERICAL SIMULATIONS

Numerical simulations of the BZ oscillator network, with topology as in Fig. 1(b), were carried out with the ZBKE model [37], modified to describe the excitatory photosensitive BZ reaction [23,34,36]. Simulations were carried out with varying coupling strength σ and oscillator frequency heterogeneity $(T_0)_{\text{std}}$, defined by the standard deviation of the period distribution of the uncoupled oscillators. The standard deviation of the mean period of the coupled oscillators was measured to determine the extent of frequency synchronization. As shown in Fig. 4(a), a sharp boundary between the synchronized and unsynchronized regions is exhibited, with the structure of a 1:1 Arnold tongue. The region inside the tongue is characterized by a vanishing standard deviation of the oscillation period over all nodes.

Another representation of the network dynamics is shown in Fig. 4(b), where the extent of phase-lag synchronization is measured, defined as the time average of the number of synchronized nodes. The 1:1 Arnold tongue continues to be apparent with this measure, and the plot contains more information about the network dynamics, including regions of partial synchronization for values of σ and $(T_0)_{\text{std}}$ that are below the full synchronization threshold.

Fully entrained states, like those found in the experiments, Figs. 1 and 2, are located inside the Arnold tongue shown in Figs. 4(a) and 4(b). The representative simulations shown in Figs. 4(c) and 4(d) are indicated in Figs. 4(a) and 4(b) by the corresponding symbols, with unsynchronized and partially synchronized behavior outside and complete phase-lag entrainment inside the Arnold tongue. As described above, fixed points corresponding to phase locking between oscillator pairs i and j disappear in saddle node bifurcations when crossing this boundary. The phase-lag synchronization therefore breaks down into partial synchronization, as shown in the second column of Figs. 4(c) and 4(d). Reducing the coupling strength further yields incoherent behavior, where all oscillator frequencies are different and are fluctuating, as shown by the frequency distribution and phases in Figs. 4(c) and 4(d), first column. The simulations also reveal new types of behavior close to the Arnold tongue boundary, Figs. 4(c) and 4(d), third column. Even though there is complete frequency locking, the phase-lag synchronization does not follow the symmetry clusters because there are inactive links in the network where the ratio of the frequency difference to the coupling strength is above the entrainment threshold. The synchronization therefore must occur via another route, where this ratio is below the threshold for every link.

For identical oscillators, phase clusters are observed rather than phase-lag synchronization, as shown in Fig. 4(b) for $(T_0)_{\text{std}} = 0$. Depending on the initial conditions, we observe either in-phase synchronization or cluster synchronization. At low coupling strength, a small degree of heterogeneity gives rise to phase-lag synchronization, and with increasing coupling strength, an increasing degree of heterogeneity is necessary for phase-lag entrainment of the network. The transition

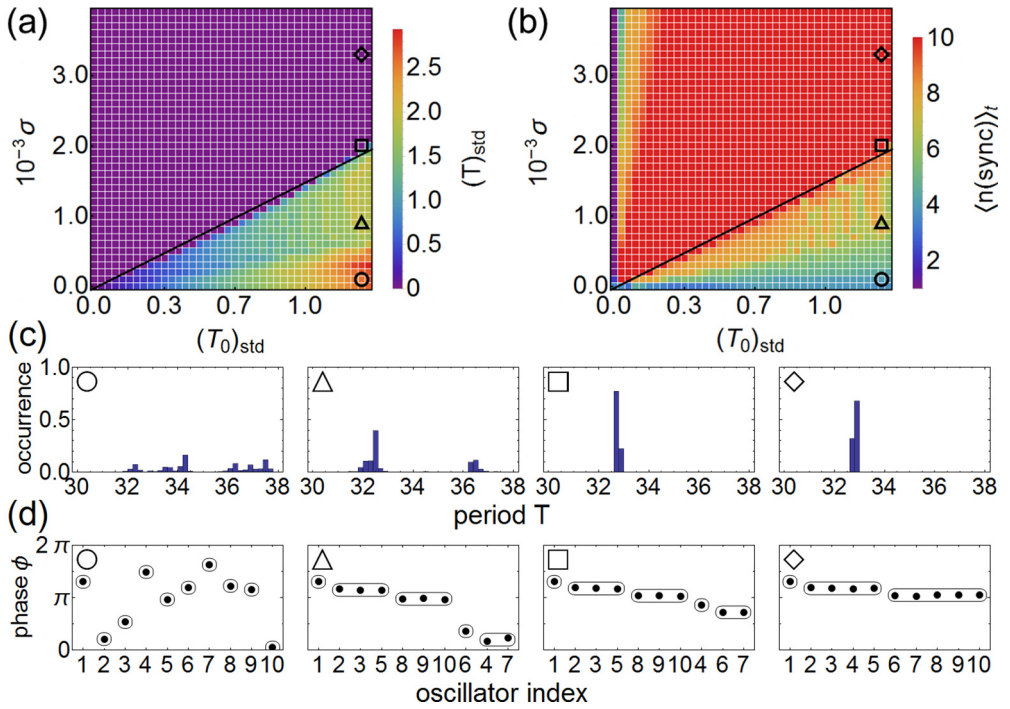

FIG. 4. (Color online) Simulations of the network of heterogeneous, photosensitive BZ oscillators with a modified ZBKE model [37]. (a) Degree of synchronization according to the standard deviation of the mean period as a function of coupling strength and the standard deviation of the uncoupled oscillator period distribution $(T_0)_{std}$. (b) The number of phase-lag synchronized oscillators, $n(\text{sync})$, as a function of coupling strength and oscillator heterogeneity defined by $(T_0)_{std}$. The number of phase-lag synchronized oscillators is determined according to $0.5 < \Delta\phi < 1.35$ for the phase difference between synchronization clusters and $\Delta\phi \leqslant 0.5$ for the phase difference within synchronization clusters. (c) and (d) Panels (left to right) showing period distribution (c) and the relative phase of each oscillator (d), corresponding to symbols in (a) and (b) for increasing coupling strength: (circle) unsynchronized, (triangle) partial synchronization, (square) full synchronization with five synchronization clusters, (diamond) full synchronization with three synchronization clusters. See the Supplemental Material [38] for modified ZBKE model and parameters.

from phase cluster synchronization, with identical oscillators, to phase-lag synchronization, with sufficient oscillator heterogeneity for a particular coupling strength, is difficult to characterize experimentally with inherently heterogeneous chemical oscillators. This transition is of significant interest and will be further explored in future computational studies.

VI. DISCUSSION

The most remarkable finding in this study is that phase-lag synchronization may occur through symmetry clusters in a network of heterogeneous BZ oscillators. In order to define the symmetry clusters in our network, we considered only the connectivity and ignored the oscillator heterogeneity, since clusters of oscillator nodes with the same permutation symmetries do not exist with heterogeneous oscillators. However, as we have described in Fig. 1, the phase-lag synchronization leads to synchronization clusters in which the oscillators are highly phase and frequency synchronized, and these synchronization clusters are made up of symmetry clusters—which have become clusters of oscillators with the same permutation symmetries. The zero-lag phase synchronization of the oscillators within a particular synchronization cluster arises from the phase-resetting character of the BZ oscillators, which can be seen from the phase-response curve of this chemical oscillator system [23]. For sufficiently high coupling strength and low frequency heterogeneity, the firing of the pacemaker, such as node 1 in Fig. 1, causes the oscillators to which it is connected to fire simultaneously, which, in this case, are nodes 2–5, with phase and frequency synchronization of these oscillators being the result. The firing of the nodes in this synchronization cluster causes the nodes to which it is connected, nodes 6–10, to fire simultaneously, again with phase and frequency synchronization being the result. The cycle then repeats, with the frequency set by the pacemaker, the first synchronization cluster. The phase lag between the first and second synchronization clusters and the second and third synchronization clusters is due to the response time of the photochemically coupled BZ oscillators. When the pacemaker fires, the oscillators at nodes 2–5 in the second synchronization cluster respond to an increase in illumination intensity with a sequence of photochemical reactions that produce the autocatalyst, $HBrO_2$ [36]. The inhibitor Br^- is consumed by the $HBrO_2$ until it reaches a critical concentration, at which point $HBrO_2$ autocatalysis rapidly occurs and the oscillators fire. A similar phase lag occurs as nodes 6–10 in the third synchronization cluster respond to the firing of the nodes in the second synchronization cluster. Hence, there is a constant phase lag in this photochemically coupled BZ oscillator network, as shown by the linear phase gradient in Fig. 1(f).

The phase-lag synchronization through symmetry clusters shown in Fig. 1 requires a pacemaker symmetry cluster

that is fully connected to one or more symmetry clusters. Typically, the pacemaker is a single oscillator node, as in Fig. 1; however, it could be a symmetry cluster made up of several oscillator nodes that are very close in frequency. If the highest frequency oscillator occurs in a symmetry cluster with other oscillators differing significantly in frequency, the phase-lag synchronization may begin without propagating through symmetry clusters, as shown in Fig. 2. We see that the pacemaker, node 1, is only half of the two-node violet symmetry cluster, and that it is also connected to node 3, which is a one-node symmetry cluster. Hence, when the pacemaker fires, it causes nodes 2 and 3 to fire synchronously, forming a synchronization cluster that is not made up of symmetry clusters. However, node 3 is fully connected to the orange symmetry cluster, made up of nodes 4 and 5. The firing of node 3 causes nodes 4 and 5 to fire synchronously, forming a synchronization cluster made up of one symmetry cluster. The orange symmetry cluster is connected to the red and light blue symmetry clusters, which then fire, forming the fourth synchronization cluster. Hence, the phase-lag synchronization through symmetry clusters is reestablished in the third and fourth synchronization clusters. Even though the phase-lag synchronization occurs only partially through symmetry clusters in this experiment, Fig. 2(b) shows that the synchronization clusters are highly phase and frequency synchronized, with the Kuramoto order parameter becoming very close to 1.0 for each cluster. We also see the constant phase lag between the firing of the nodes in each synchronization cluster in Fig. 2(c), with a linear phase gradient.

In this paper, we have shown that networks of heterogeneous chemical oscillators synchronize by phase-lag synchronization through synchronization clusters made up of symmetry clusters for sufficiently high coupling strength and low heterogeneity. As discussed above, the location of the pacemaker also plays an important role in this behavior. The synchronization clusters exhibit a high degree of phase and frequency synchronization even though they contain oscillators with a range of natural frequencies. A constant phase lag is exhibited between the firing of successive synchronization clusters, which arises from the chemical response time of the photochemically coupled oscillators. The frequency of the network is set by the pacemaker, which is typically a single oscillator with the highest frequency. The pacemaker may be a multiple-node symmetry cluster if the oscillators in the cluster have nearly the same frequency. However, a multiple-node symmetry cluster containing a single node pacemaker may lead to phase-lag synchronization that occurs only partially through symmetry clusters.

We have found that the shortest path from the pacemaker to the final synchronization cluster, which corresponds to one full oscillation of the network, occurs with phase-lag synchronization through symmetry clusters. We use the adjacency matrix to derive the distance matrix of the network. Its elements are the shortest paths as computed by Dijkstra's algorithm [44] between any nodes i and j, with i,j ranging from 1 to N. In networks with phase-lag synchronization, the algorithm follows the path of successive synchronization clusters made up of symmetry clusters. Phase-lag synchronization that occurs partially through symmetry clusters typically has one or more additional synchronization clusters, such as the example in Fig. 2 or in Fig. 4(d), third column. Hence, if one considers the phase-lag synchronization of a network as a means of information transfer through the network, the phase-lag synchronization through symmetry clusters would be the fastest.

Phase-lag synchronization in our network of coupled heterogeneous chemical oscillators propagates through synchronization clusters much like synchronization by a phase wave. A possible benefit of synchronization clusters is that they provide a redundancy of nodes if one or more nodes in the cluster cannot be synchronized. This redundancy may result in an increased robustness of phase-lag synchronization in natural systems with inherent heterogeneity. Phase synchronization is thought to play a key role in neural communication between regions of the brain [45], and phase-lag synchronization is a possible mechanism for such processes [46,47]. However, zero-lag synchronization is also found in the brain [48,49], and how each of these processes occur remains an open question. We hope that studies of simple physical systems such as networks of coupled chemical oscillators can offer insights into the possible mechanisms of biological signal transmission in neural communication [45] as well as central pattern generators [14].

ACKNOWLEDGMENTS

We are grateful to Louis M. Pecora for early and insightful discussions and for providing prepublication of a manuscript. J.F.T. and H.E. thank the German Science Foundation (DFG) for financial support through the Sonderforschungsbereich (SFB 910). R.S. thanks the Cultural Mission of the Royal Embassy of Saudi Arabia for a Ph.D. scholarship. K.S. thanks the Alexander von Humboldt Foundation for supporting a research visit at Technical University Berlin and is grateful to Harald Engel and Eckehard Schöll for their hospitality and productive research collaboration. This material is based on work supported by the National Science Foundation (Grant No. CHE-1212558).

[1] A. T. Winfree, *The Geometry of Biological Time* (Springer, New York, 2001).
[2] Y. Kuramoto, *Chemical Oscillations, Waves, and Turbulence* (Courier Dover Publications, Mineola, 2003).
[3] A. Pikovsky, M. Rosenblum, and J. Kurths, *Synchronization: A Universal Concept in Nonlinear Sciences* (Cambridge University Press, Cambridge, 2003).
[4] S. H. Strogatz, Nature (London) **410**, 268 (2001).
[5] R. Albert and A.-L. Barabási, Rev. Mod. Phys. **74**, 47 (2002).
[6] A. Arenas, A. Daz-Guilera, J. Kurths, Y. Moreno, and C. Zhou, Phys. Rep. **469**, 93 (2008).
[7] S. Boccaletti, V. Latora, Y. Moreno, M. Chavez, and D. U. Hwang, Phys. Rep. **424**, 175 (2006).
[8] S. H. Strogatz, Physica D **143**, 1 (2000).

[9] F. Dörfler and F. Bullo, Automatica **50**, 1539 (2014).
[10] J. Gómez-Gardeñes, S. Gómez, A. Arenas, and Y. Moreno, Phys. Rev. Lett. **106**, 128701 (2011).
[11] P. S. Skardal, J. Sun, D. Taylor, and J. G. Restrepo, Europhys. Lett. **101**, 20001 (2013).
[12] P. S. Skardal, D. Taylor, and J. Sun, Phys. Rev. Lett. **113**, 144101 (2014).
[13] M. I. Rabinovich, P. Varona, A. I. Selverston, and H. D. I. Abarbanel, Rev. Mod. Phys. **78**, 1213 (2006).
[14] E. Marder and D. Bucher, Curr. Biol. **11**, R986 (2001).
[15] A. H. Cohen, B. G. Ermentrout, T. Kiemel, N. Kopell, K. A. Sigvardt, and T. L. Williams, Trends Neurosci. **15**, 434 (1992).
[16] B. Ravoori, A. B. Cohen, J. Sun, A. E. Motter, T. E. Murphy, and R. Roy, Phys. Rev. Lett. **107**, 034102 (2011).
[17] C. R. S. Williams, F. Sorrentino, T. E. Murphy, and R. Roy, Chaos **23**, 043117 (2013).
[18] A. M. Hagerstrom, T. E. Murphy, R. Roy, P. Hövel, I. Omelchenko, and E. Schöll, Nat. Phys. **8**, 658 (2012).
[19] Y. Jia and I. Z. Kiss, J. Phys. Chem. C **116**, 19290 (2012).
[20] M. Wickramasinghe and I. Z. Kiss, PLoS One **8**, e80586 (2013).
[21] M. Wickramasinghe and I. Z. Kiss, Phys. Chem. Chem. Phys. **16**, 18360 (2014).
[22] V. Horvath, P. L. Gentili, V. K. Vanag, and I. R. Epstein, Angew. Chem. Intern. Ed. **51**, 6878 (2012).
[23] M. R. Tinsley, S. Nkomo, and K. Showalter, Nat. Phys. **8**, 662 (2012).
[24] S. Nkomo, M. R. Tinsley, and K. Showalter, Phys. Rev. Lett. **110**, 244102 (2013).
[25] N. Tompkins, N. Li, C. Girabawe, M. Heymann, G. B. Ermentrout, I. R. Epstein, and S. Fraden, Proc. Nation. Acad. Sci. USA **111**, 4397 (2014).
[26] L. M. Pecora, F. Sorrentino, A. M. Hagerstrom, T. E. Murphy, and R. Roy, Nat. Commun. **5**, 4079 (2014).
[27] A. N. Zaikin and A. M. Zhabotinsky, Nature (London) **225**, 535 (1970).
[28] J. Maselko and K. Showalter, Nature (London) **339**, 609 (1989).
[29] H. Fukuda, N. Tamari, H. Morimura, and S. Kai, J. Phys. Chem. A **109**, 11250 (2005).
[30] A. F. Taylor, M. R. Tinsley, F. Wang, Z. Huang, and K. Showalter, Science **323**, 614 (2009).
[31] A. F. Taylor, M. R. Tinsley, F. Wang, and K. Showalter, Angew. Chem. Intern. Ed. **123**, 10343 (2011).
[32] V. Gáspár, G. Basza, and M. T. Beck, Z. Phys. Chem. (Leipzig) **264**, 43 (1983).
[33] L. Kuhnert, Nature (London) **319**, 393 (1986).
[34] A. F. Taylor, P. Kapetanopoulos, B. J. Whitaker, R. Toth, L. Bull, and M. R. Tinsley, Phys. Rev. Lett. **100**, 214101 (2008).
[35] K. Kalyanasundaram, Coord. Chem. Rev. **46**, 159 (1982).
[36] S. Kádár, T. Amemiya, and K. Showalter, J. Phys. Chem. A **101**, 8200 (1997).
[37] A. M. Zhabotinsky, F. Buchholtz, A. B. Kiyatkin, and I. R. Epstein, J. Phys. Chem. **97**, 7578 (1993).
[38] See Supplemental Material at http://link.aps.org/supplemental/10.1103/PhysRevE.92.022819 for experimental setup, numerical model, and other network topologies.
[39] O.-U. Kheowan, E. Mihaliuk, B. Blasius, I. Sendiña-Nadal, and K. Showalter, Phys. Rev. Lett. **98**, 074101 (2007).
[40] P. C. Matthews and S. H. Strogatz, Phys. Rev. Lett. **65**, 1701 (1990).
[41] D. Garlaschelli, F. Ruzzenenti, and R. Basosi, Symmetry **2**, 1683 (2010).
[42] The GAP Group. GAP: Groups, Algorithms, and Programming, Version 4-4 (http://www.gap-system.org, 2005).
[43] H. Kori and A. S. Mikhailov, Phys. Rev. E **74**, 066115 (2006).
[44] E. W. Dijkstra, Numer. Math. **1**, 269 (1959).
[45] J. Fell and N. Axmacher, Nat. Rev. Neurosci. **12**, 105 (2011).
[46] G. G. Gregoriou, S. J. Gotts, H. H. Zhou, and R. Desimone, Science **324**, 1207 (2009).
[47] K. Benchenane, A. Peyrache, M. Khamassi, P. L. Tierney, Y. Gioanni, F. P. Battaglia, and S. I. Wiener, Neuron **66**, 921 (2010).
[48] J. Fell, P. Klaver, K. Lehnertz, T. Grunwald, C. Schaller, C. E. Elger, and G. Fernandez, Nat. Neurosci. **4**, 1259 (2001).
[49] T. Seidenbecher, T. R. Laxmi, O. Stork, and H. C. Pape, Science **301**, 846 (2003).

Supplemental Material
for
Phase-lag synchronization in networks of coupled chemical oscillators

Jan F. Totz,[1] Razan Snari,[2] Desmond Yengi,[2] Mark R. Tinsley,[2] Harald Engel,[1] and Kenneth Showalter[2,*]

[1] *Institut für Theoretische Physik, EW 7-1, TU Berlin, Hardenbergstr. 36, 10623 Berlin, Germany*

[2] *C. Eugene Bennett Department of Chemistry, West Virginia University, Morgantown, West Virginia 26505-6045, USA*

CONTENTS

A. EXPERIMENTAL SETUP

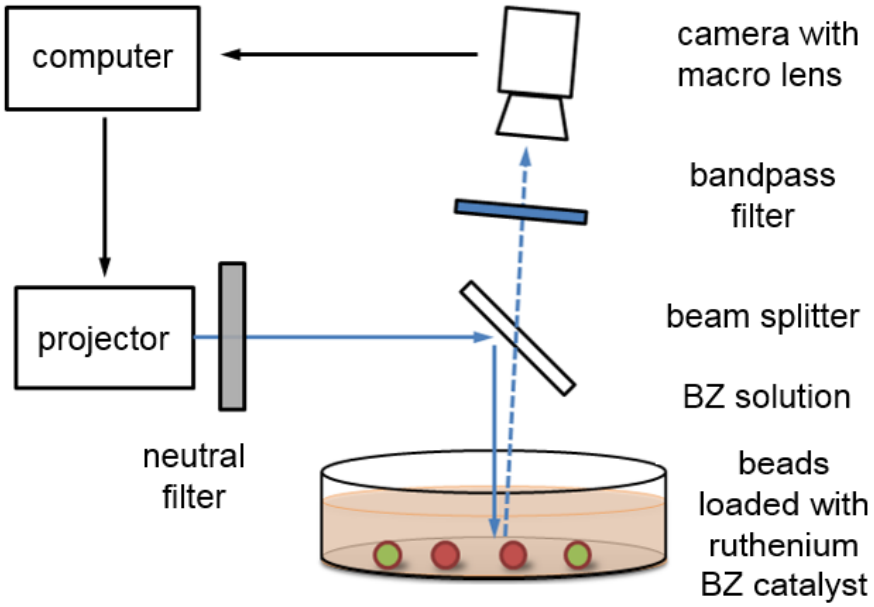

FIG. 1. Schematic drawing of the experimental setup.

Catalyst-loaded cation-exchange beads (DOWEX, mesh 50) are placed in catalyst-free Belousov-Zhabotinsky (BZ) reaction mixtures. During an oscillation cycle, the beads change color based on the concentrations of the reduced and oxidized forms of the BZ catalyst, $Ru(bipy)_3^{2+}$ (orange) and $Ru(bipy)_3^{3+}$ (green), respectively. The color changes are measured in gray scale images with a CCD camera. A bandpass filter improves the contrast of the gray scale signal due to the respective extinction coefficients of the reduced and oxidized forms of the BZ catalyst at 440-460 nm.

The photochemical coupling between two oscillators i and j is carried out by determining the difference in the transmitted light intensity, in gray scale, and multiplying this difference by the normalized coupling constant according to Eq. (1) in Totz et al. (or Eq. (1) below). The light intensity ϕ_i projected on oscillator i with an SLM generates the excited form of the reduced catalyst, $Ru(bipy)_3^{2+*}$. The excited catalyst reacts directly with the reactant BrO_3^-, and in a series of subsequent reactions produces the autocatalyst $HBrO_2$. Additional $HBrO_2$ typically results in a phase advance in the excitatory BZ reaction, although there is little effect during the excited or recovery period [1–3].

The normalized gray scale values z_j and z_i, which are proportional to the $Ru(bipy)_3^{3+}$ concentration, the normalized coupling constant σ, and the projected and background light

intensities, ϕ_i and ϕ_0, in Eq. (1) are dimensionless. The value of ϕ_0 is equal to 0.47, and the actual value of the applied light intensity can be calculated by multiplying the dimensionless light intensity ϕ by 3.0 mW cm^{-2}. The experimental time for determining the gray level of oscillator j and projecting the light intensity ϕ_i on oscillator i is approximately 0.4 s.

TABLE I. Initial concentrations for catalyst-free solution and catalyst-loaded beads

MA	0.08 M
H_2SO_4	0.78 M
NaBr	0.02 M
$NaBrO_3$	0.48 M
$Ru(bipy)_3^{2+}$	8.3×10^{-6} mol/g

B. NUMERICAL MODEL

The chemical reaction taking place on each catalyst-loaded bead and the influence of the projected light perturbations on the reaction are simulated with a dimensionless modified ZBKE model for the photosensitive BZ reaction [2–4].

$$\phi_i = \phi_0 + \frac{\sigma}{k_i}\sum_{j=1}^{N} A_{ij}(z_j - z_i) \tag{1}$$

$$u_{ss,i}(x_i, z_i) = \frac{1}{4\gamma\epsilon_2}\left(\sqrt{16\gamma x_i\epsilon_2 + z_i^2 - 2z_i + 1} + z_i - 1\right) \tag{2}$$

$$\dot{x_i}(x_i, z_i) = \frac{1}{\epsilon_1}\left(\phi_i + \frac{\mu - x_i}{\mu + x_i}\left(\beta + \frac{\alpha q_i z_i}{\epsilon_3 + 1 - z_i}\right) + \gamma\epsilon_2 u_{ss,i}^2 + (1 - z_i)u_{ss,i} - x_i^2 - x_i\right) \tag{3}$$

$$\dot{z_i}(x_i, z_i) = \phi_i + (1 - z_i)u_{ss,i} - \frac{\alpha z_i}{\epsilon_3 + 1 - z_i} \tag{4}$$

Variable definitions and parameter values are given in the following table:

TABLE II. Model information

$x_i(t)$		$[HBrO_2]$
$z_i(t)$		$[Ru(bipy)_3^{3+}]$
$u_{ss,i}(x_i, z_i)$		steady state $[HBrO_2^+]$
ϕ_i		light intensity projected on node i
σ		coupling strength
k_i		degree of node i
A_{ij}		adjacency matrix element
ϵ_1	0.11	time scale parameters
ϵ_2	1.7×10^{-5}	
ϵ_3	1.6×10^{-3}	
q_i	$0.5 - 1.0$	stoichiometric parameter
α	0.1	kinetic parameters
β	1.7×10^{-5}	
γ	1.2	
μ	2.4×10^{-4}	
ϕ_0	1.6×10^{-4}	background light intensity

C. PHASE-LAG SYNCHRONIZATION WITH OTHER NETWORK TOPOLOGIES

The phase-lag synchronization is not restricted to the network topology presented in Figs. 1 - 4, Totz et al. We show here that phase-lag synchronization occurs when nodes are added to the original network topology, with one node added in Fig. 2, and with the original network topology duplicated and connected in Fig. 3. With more nodes, we observe more synchronization clusters and, in turn, a larger gap between the Kuramoto order parameter of the complete network and of the synchronization clusters. A linear phase gradient between the synchronization clusters, with a slope of approximately -0.31, illustrates a constant phase shift between adjacent synchronization clusters in the networks shown in Figs. 2 and 3. We also found phase lag-synchronization in simulations of other classes of networks, such as the densely connected random network [5] in Fig. 4 and a random scale-free network based on the Barabási-Albert algorithm [6] in Fig. 5. We find that the synchronization clusters and symmetry clusters are identical in a ternary tree network [7], shown in Fig. 6. All of the examples shown here exhibit synchronization clusters that follow the symmetry clusters of the network topology.

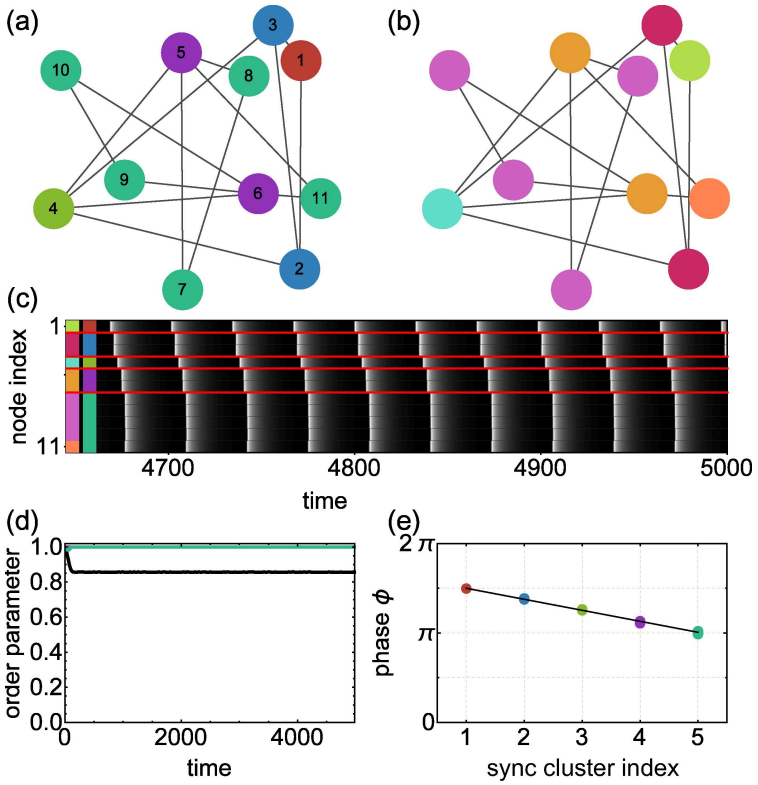

FIG. 2. Simulations of phase-lag synchronization in a network of heterogeneous, photosensitive Belousov-Zhabotinsky (BZ) chemical oscillators with the modified ZBKE model [2–4]. The network is the same as that presented in Figs. 1 - 4, Totz et al. except that it has one additional node (number 11). (a) The bidirectional links show the connectivity in the network. Nodes that oscillate simultaneously, or nearly so, are the same color and define a *synchronization cluster*. (b) The symmetry clusters of the network, where the nodes in each symmetry cluster are the same color. (c) Value of the variable z_i in the ZBKE model as a function of time for each node i, with the black and white color code corresponding to low and high values, respectively. The node index corresponds to the numbering in (a). Red lines separate the groups of synchronized nodes from each other, with synchronized nodes and symmetry clusters color coded as in (a) and (b), respectively. (d) Kuramoto order parameter [8] for each synchronization cluster, color coded as in (a), and the complete network (black) as a function of time. The order parameter values for the synchronization clusters approach unity and overlap. (e) A linear fit through the phase occurrence of each node of each synchronization cluster reveals a constant phase gradient (color coding as in (a)). The coupling strength is $\sigma = 0.0039$; the mean natural period and standard deviation is $T_0 = 35.54 \pm 1.26$; see Section B for other parameters.

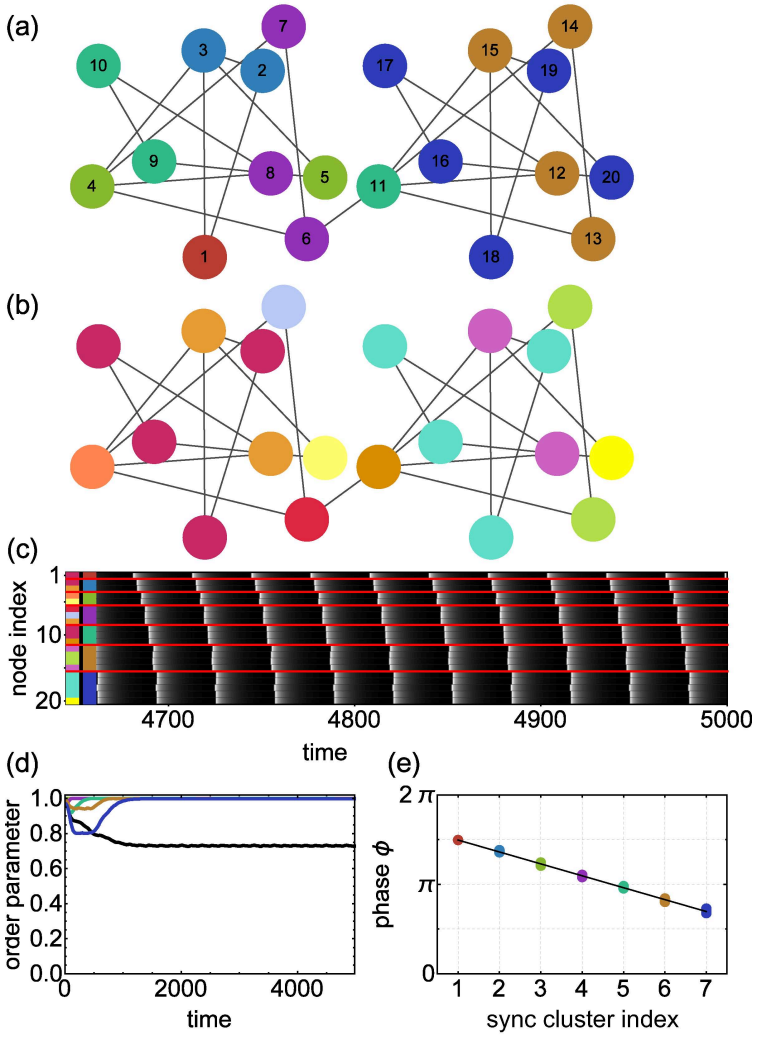

FIG. 3. Simulations of phase-lag synchronization in a network of heterogeneous, photosensitive BZ chemical oscillators with the modified ZBKE model [2–4]. The network is made up of two connected copies of the network presented in Figs. 1 - 4, Totz et al. (a) The bidirectional links show the connectivity; nodes that oscillate simultaneously are the same color and define a *synchronization cluster*. (b) The symmetry clusters of the network, where the nodes in each symmetry cluster are the same color. (c) Value of the variable z_i in the ZBKE model as a function of time for each node i, with the black and white color code corresponding to low and high values, respectively. (d) Kuramoto order parameter [8] for each synchronization cluster, color coded as in (a), and the complete network (black) as a function of time. (e) A linear fit through the phase occurrence of each node of each synchronization cluster reveals a constant phase gradient (color coding as in (a)). The coupling strength is $\sigma = 0.0039$; the mean natural period and standard deviation is $T_0 = 35.54 \pm 1.26$; see Section B for other parameters.

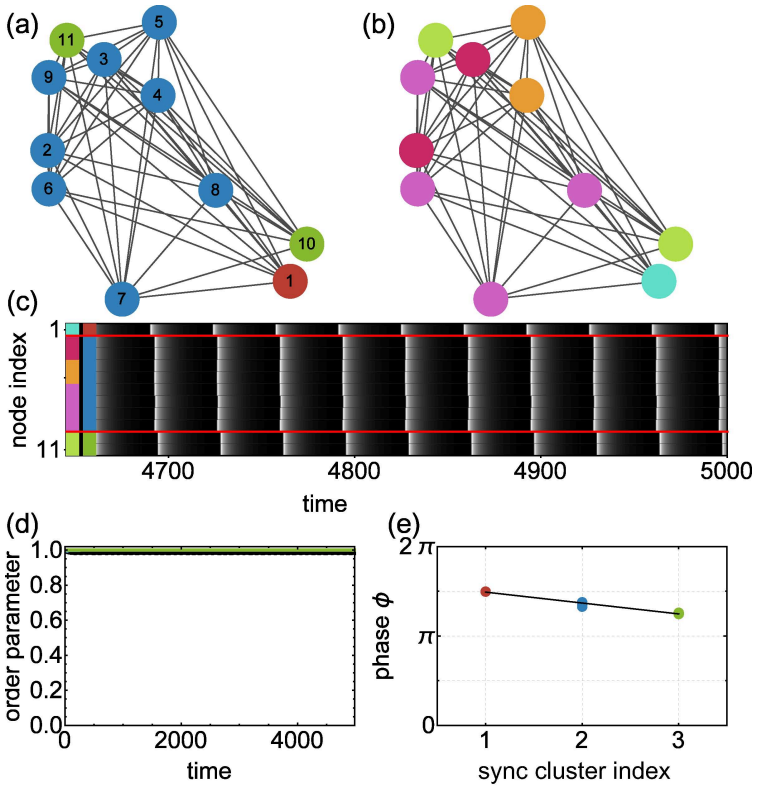

FIG. 4. Simulations of phase-lag synchronization in a random densely connected network with 11 nodes, as in [5], of heterogeneous, photosensitive BZ chemical oscillators with the modified ZBKE model [2–4]. (a) The bidirectional links show the connectivity; nodes that oscillate simultaneously are the same color and define a *synchronization cluster*. (b) The symmetry clusters of the network, where the nodes in each symmetry cluster are the same color. (c) Value of the variable z_i in the ZBKE model as a function of time for each node i, with the black and white color code corresponding to low and high values, respectively. (d) Kuramoto order parameter [8] for each synchronization cluster, color coded as in (a), and the complete network (black) as a function of time. (e) A linear fit through the phase occurrence of each node of each synchronization cluster reveals a constant phase gradient (color coding as in (a)). The coupling strength is $\sigma = 0.0039$; the mean natural period and standard deviation is $T_0 = 35.54 \pm 0.95$; see Section B for other parameters.

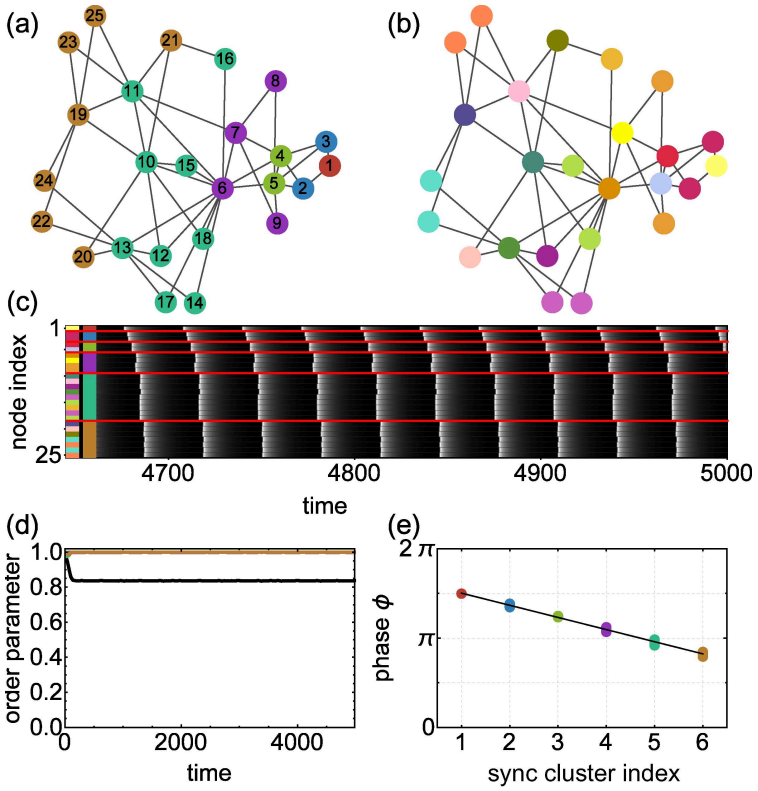

FIG. 5. Simulations of phase-lag synchronization in a random scale-free network [6] with 25 nodes of heterogeneous, photosensitive BZ chemical oscillators with the modified ZBKE model [2–4]. (a) The bidirectional links show the connectivity; nodes that oscillate simultaneously are the same color and define a *synchronization cluster*. (b) The symmetry clusters of the network, where the nodes in each symmetry cluster are the same color. (c) Value of the variable z_i in the ZBKE model as a function of time for each node i, with the black and white color code corresponding to low and high values, respectively. (d) Kuramoto order parameter [8] for each synchronization cluster, color coded as in (a), and the complete network (black) as a function of time. (e) A linear fit through the phase occurrence of each node of each synchronization cluster reveals a constant phase gradient (color coding as in (a)). The coupling strength is $\sigma = 0.0039$; the mean natural period and standard deviation is $T_0 = 35.54 \pm 1.26$; see Section B for other parameters.

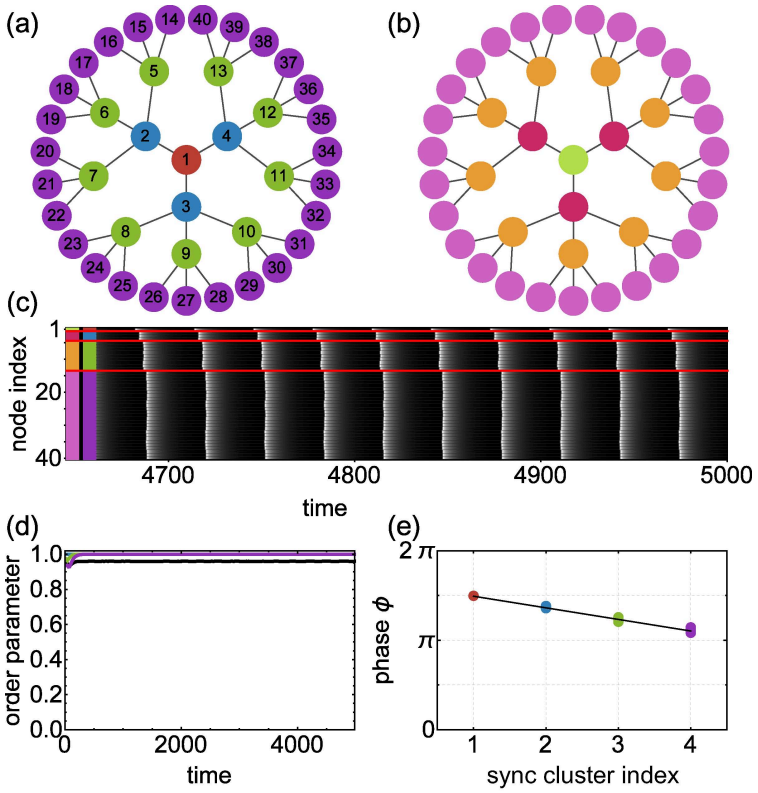

FIG. 6. Simulations of phase-lag synchronization in a ternary tree network [7] with 40 nodes of heterogeneous, photosensitive BZ chemical oscillators with the modified ZBKE model [2–4]. (a) The bidirectional links show the connectivity; nodes that oscillate simultaneously are the same color and define a *synchronization cluster*. (b) The symmetry clusters of the network, where the nodes in each symmetry cluster are the same color. (c) Value of the variable z_i in the ZBKE model as a function of time for each node i, with the black and white color code corresponding to low and high values, respectively. (d) Kuramoto order parameter [8] for each synchronization cluster, color coded as in (a), and the complete network (black) as a function of time. (e) A linear fit through the phase occurrence of each node of each synchronization cluster reveals a constant phase gradient (color coding as in (a)). The coupling strength is $\sigma = 0.0039$; the mean natural period and standard deviation is $T_0 = 35.54 \pm 1.26$; see Section B for other parameters.

D. MEAN UNCOUPLED OSCILLATOR PERIOD AND SYNCHRONIZED NETWORK PERIOD

We consider 5 different frequency distributions on the network of oscillators shown on Fig. 1(a), Totz et al., corresponding to the simulations in Fig. 4, Totz et al. The highest frequency oscillator is assigned to node 1 in Fig. 1(a).

The table below shows the uncoupled and coupled mean period and standard deviation of the entire network, $(T)_{mean}$, and the mean period and corresponding standard deviation of the i'th synchronization cluster, $(T_i)_{mean}$. The first synchronization cluster is given by the pacemaker. Note that in the coupled case the standard deviation vanishes, as all nodes are synchronized. In all cases, the period of the network is within 1% of the natural (uncoupled) period of the pacemaker.

uncoupled				coupled	
$(T)_{mean}$	$(T_1)_{mean}$	$(T_2)_{mean}$	$(T_3)_{mean}$	$(T)_{mean}$	$(T_1)_{mean}$
36.20 ± 2.65	32.17 ± 0.00	36.39 ± 3.03	36.84 ± 2.07	32.35 ± 0.00	32.35 ± 0.00
36.62 ± 4.21	31.89 ± 0.00	36.34 ± 3.55	37.79 ± 4.81	32.07 ± 0.00	32.07 ± 0.00
35.35 ± 2.22	32.40 ± 0.00	35.20 ± 2.94	36.06 ± 1.32	32.55 ± 0.00	32.55 ± 0.00
34.90 ± 1.93	32.11 ± 0.00	35.39 ± 2.01	35.07 ± 1.78	32.28 ± 0.00	32.28 ± 0.00
36.38 ± 1.81	32.63 ± 0.00	37.56 ± 1.43	36.18 ± 0.93	32.83 ± 0.00	32.83 ± 0.00

* kenneth.showalter@mail.wvu.edu

[1] S. Kádár, T. Amemiya, and K. Showalter, J. Phys. Chem. A **101**, 8200 (1997).

[2] A. F. Taylor, P. Kapetanopoulos, B. J. Whitaker, R. Toth, L. Bull, and M. R. Tinsley, Phys. Rev. Lett. **100**, 214101 (2008).

[3] M. R. Tinsley, S. Nkomo, and K. Showalter, Nat. Phys. **8**, 662 (2012).

[4] A. M. Zhabotinsky, F. Buchholtz, A. B. Kiyatkin, and I. R. Epstein, J. Phys. Chem. **97**, 7578 (1993).

[5] L. M. Pecora, F. Sorrentino, A. M. Hagerstrom, T. E. Murphy, and R. Roy, Nat. Commun. **5**, 4079 (2014).

[6] A.-L. Barabási and R. Albert, Science **286**, 509 (1999).

[7] D. E. Knuth, *The Art of Computer Programming: Fundamental algorithms*, Vol. 1 (Addison-Wesley, 1997).

[8] Y. Kuramoto, *Chemical Oscillations, Waves, and Turbulence* (Courier Dover Publications, 2003).